Impact of Winter Ural Blocking on Arctic Sea Ice: Short-Time Variability

XIAODAN CHEN

CAS Key Laboratory of Regional Climate-Environment for Temperate East Asia, Institute of Atmospheric Physics, Chinese Academy of Sciences, and University of Chinese Academy of Sciences, Beijing, China

Dehai Luo

CAS Key Laboratory of Regional Climate-Environment for Temperate East Asia, Institute of Atmospheric Physics, Chinese Academy of Sciences, and University of Chinese Academy of Sciences, Beijing, and Ningbo Collaborative Innovation Center of Nonlinear Hazard System of Ocean and Atmosphere, Ningbo University, Ningbo, China

STEVEN B. FELDSTEIN AND SUKYOUNG LEE

Department of Meteorology and Atmospheric Science, The Pennsylvania State University, University Park, Pennsylvania

(Manuscript received 24 March 2017, in final form 12 December 2017)

ABSTRACT

Using daily reanalysis data from 1979 to 2015, this paper examines the impact of winter Ural blocking (UB) on winter Arctic sea ice concentration (SIC) change over the Barents and Kara Seas (BKS). A case study of the sea ice variability in the BKS in the 2015/16 and 2016/17 winters is first presented to establish a link between the BKS sea ice variability and UB events. Then the UB events are classified into quasi-stationary (QUB), westward-shifting (WUB), and eastward-shifting (EUB) UB types. It is found that the frequency of the QUB events increases significantly during 1999–2015, whereas the WUB events show a decreasing frequency trend during 1979–2015.

Moreover, it is shown that the variation of the BKS-SIC is related to downward infrared radiation (IR) and surface sensible and latent heat flux changes due to different zonal movements of the UB. Calculations show that the downward IR is the main driver of the BKS-SIC decline for QUB events, while the downward IR and surface sensible heat flux make comparable contributions to the BKS-SIC variation for WUB and EUB events. The SIC decline peak lags the QUB and EUB peaks by about 3 days, though QUB and EUB require lesser prior SIC. The QUB gives rise to the largest SIC decline likely because of its longer persistence, whereas the BKS-SIC decline is relatively weak for the EUB. The WUB is found to cause a SIC decline during its growth phase and an increase during its decay phase. Thus, the zonal movement of the UB has an important impact on the SIC variability in BKS.

1. Introduction

Over the past decade, Arctic sea ice extent has been observed to undergo a marked decline since the early 2000s (Comiso 2006; Francis and Hunter 2007; Screen and Simmonds 2010a,b; Simmonds 2015). Because Northern Hemisphere midlatitude extreme cold events in winter (Screen and Simmonds 2013a,b; Cohen et al. 2014), habitat ecosystems (Forbes et al. 2016), and increased coastal erosion and changes to the ocean circulation have been shown to be closely related to rapid Arctic sea ice decline and Arctic warming (Overland et al. 2011, 2015; Walsh 2014; Mori et al. 2014) linked to

Corresponding author: Dr. Dehai Luo, ldh@mail.iap.ac.cn

winter Ural blocking (Luo et al. 2016a,b; D. Luo et al. 2017; Gong and Luo 2017), the physical cause of this rapid decline of Arctic sea ice during the past decade has been a research topic of great interest (D.-S. R. Park et al. 2015; H.-S. Park et al. 2015; Gong and Luo 2017; Gong et al. 2017; Lee et al. 2017).

During the past two decades, several hypotheses have been proposed to explain the decline in Arctic sea ice (Fang and Wallace 1994; Francis and Hunter 2007; Screen and Simmonds 2010a; D.-S. R. Park et al. 2015). For example, the enhanced inflow of warm Pacific and Atlantic water into the Arctic (Shimada et al. 2006; Spielhagen et al. 2011) and the increased sea surface temperature (SST) over the Arctic (Comiso 2006; Francis and Hunter 2007) have been shown to

contribute to Arctic sea ice loss. On both intraseasonal and interannual time scales, recent studies also revealed that enhanced downward infrared radiation (IR) is important for the recent winter Arctic sea ice loss, whereas the surface sensible heat flux plays a minor role (Doyle et al. 2011; Woods et al. 2013; D.-S. R. Park et al. 2015; H.-S. Park et al. 2015; Gong et al. 2017; B. Luo et al. 2017). Many studies have shown that the intensified downward IR arises from an enhanced poleward transport of warm and moist air to the Arctic (Doyle et al. 2011; Yoo et al. 2012a,b; Ghatak and Miller 2013; Woods et al. 2013; D.-S. R. Park et al. 2015; H.-S. Park et al. 2015; Baggett et al. 2016; Woods and Caballero 2016; B. Luo et al. 2017; Gong et al. 2017). In particular, Woods et al. (2013) showed that the enhanced poleward moisture intrusion is often located on the western side of a blocking anticyclone. A recent study indicated that the enhanced frequency of Ural blocking (UB) events in high latitudes during 2000-13 is associated with an interannual warming over the Barents and Kara Seas (BKS; 65°-80°N, 30°-90°E) (Luo et al. 2016a,b). The BKS ice reduction is found to coincide with a UB pattern and the positive North Atlantic Oscillation (NAO⁺; Luo et al. 2016a; Gong and Luo 2017), while the UB arises from the decay of the NAO⁺ through large-scale wave train propagation (Luo et al. 2016b). In contrast, the winter sea ice decline in the Labrador Sea occurs together with the negative North Atlantic Oscillation (NAO⁻). Gong and Luo (2017) further found that on the intraseasonal time scale the UB can amplify the sea ice decline over the BKS as it occurs together with the NAO⁺, and that the reduced sea ice over the BKS, which persists for several weeks, lags the UB by about 4 days. B. Luo et al. (2017) presented an explanation for why the strongest BKS ice decline is closely related to the combined UB and NAO⁺. They found that the UB with NAO⁺ is an optimal circulation pattern that favors the intrusion of midlatitude warm moisture in the Gulf Stream Extension region into the BKS to produce strong BKS warming and sea ice reduction through intensifying the migration of cyclones from the North Atlantic midlatitudes to the BKS. Thus, these results suggest that the UB is able to exert a large effect on the Arctic sea ice reduction over the BKS through changes in water vapor. While the winter sea ice extent variability is dominated by changes in the sea ice condition in the BKS (B. Luo et al. 2017; Gong and Luo 2017), examining the processes that cause these large sea ice changes can help to understand the cause of winter sea ice coverage loss and perhaps help sea ice extent predictions. Furthermore, as noted in a recent study (Yao et al. 2017), the precise longitudinal position of the UB has an important impact on winter Arctic warming over the BKS. This motivates

us to categorize UB events by their longitudinal movement, and then to examine how the UB movement affects winter Arctic sea ice variability. On this basis, we present the new finding that the quasi-stationary UB can lead to the strongest sea ice decline in BKS compared to eastward- and westward-moving UB events and the rapid decline of the winter BKS sea ice observed during 1999–2015 is closely related to the increased frequency of quasi-stationary UB events.

This paper is organized as follows: In section 2, we describe the data and method. In section 3, a case study of winter sea ice variability is presented for two recent winters, 2015/16 and 2016/17, to demonstrate the likely role of UB events for the variability of BKS winter sea ice. In section 4, we provide observational evidence to indicate that strong Arctic sea ice loss over the BKS is closely related to quasi-stationary UB patterns. Moreover, we examine how the movement of the UB affects the variability of Arctic sea ice over the BKS in section 5. The conclusions and a discussion are presented in section 6.

2. Data and method

We use daily SIC data for the winter [December-February (DJF)] from the National Snow and Ice Data Center (NSIDC), for the time period ranging from December 1979 to February 2015 (http://nsidc.org/data/ seaice_index/). Because of missing SIC data, our analysis excludes the time period from December 1987 to February 1988. In addition, daily ERA-Interim SIC data for five months from November to March (NDJFM) during 2015/16 and 2016/17 is also used to perform our case analysis (Dee et al. 2011) because the NSIDC sea ice data cannot be obtained during the period of performing this case study and there is a consistent result between the NSIDC and ERA-interim SIC datasets (D.-S. R. Park et al. 2015). We also use daily 500-hPa geopotential height, zonal wind, surface air temperature, downward IR, and surface and latent heat flux data taken from the National Centers for Environmental Prediction (NCEP)-National Center for Atmospheric Research (NCAR) reanalysis dataset for 1979–2015 (Kalnay et al. 1996; http://www.esrl.noaa.gov/psd/). The anomaly at each grid point during 1979-2015 is calculated as a deviation from its long time mean (1979–2015) for each day of the winter. Furthermore, the anomaly is linearly detrended and deseasonalized for the time period 1979–2015.

To identify Ural blocking events, the blocking index of Tibaldi and Molteni (1990) is used, which is referred to as the TM index (Luo et al. 2016a). This index is based on the meridional gradient of 500-hPa geopotential

height at three reference latitudes. The details of this index definition can be found in Tibaldi and Molteni (1990) and Luo et al. (2016a). We use a 5-day moving average to smooth the high-frequency variability before calculating the blocking index. A blocking event is determined to have occurred if the instantaneous blocking lasts for at least three consecutive days. We define the domain for a UB event as 30°-90°E. The duration of a UB event is defined to be the persistence time of the UB that satisfies the criterion of the TM index (Luo et al. 2016a; Yao et al. 2017). Here, we use a Monte Carlo simulation to test the statistical significance of the difference between two composites or for a single composite when the sample size (number) is smaller and does not satisfy a normal distribution (Wilks 2011). When the sample size is sufficiently large, a Student's t test is used if the sample distribution resembles a normal distribution (Von Storch and Zwiers 2001).

We define a quasi-stationary UB (QUB) to have taken place if the anticyclonic center of the blocking event remains over the Ural region (from 30° to 90°E) throughout the life cycle of the blocking event. Eastward-(EUB) or westward-shifted (WUB) UB events are identified by an anticyclonic center that is initially within the Ural region and then moves outside the Ural region toward the east or west of the QUB domain, respectively, during its life cycle.

3. A case study of the influence of Ural blocking on winter BKS sea ice change

The decrease in sea ice extent in late December through early January 2015/16 is also attributed to an extreme cyclone in that region that caused sea ice melting (Boisvert et al. 2016). But the movement and direction of extreme cyclones in high latitudes are actually modulated by large-scale circulation patterns such as blocking flows. Thus, synoptic cyclones entering the BKS are related to the presence of UB.

To investigate whether the UB significantly affects BKS winter sea ice, it is useful to perform a case analysis of the sea ice changes in the BKS during two recent winter seasons. We first show the monthly-mean SIC anomaly patterns around the Arctic from November to March for the 2015/16 and 2016/17 winters in Fig. 1a and the daily time series of the NDJFM SIC anomalies averaged in the BKS (65°–85°N, 30°–90°E) in Fig. 1b. It is interesting to see that whereas the negative SIC anomaly in November is smaller for 2015 than for 2016, the SIC maintains its large negative anomaly through to the following February and March of the 2015/16 winter (Fig. 1a). To some extent, the large difference of the BKS SIC anomaly between the two winters is likely

related to the difference in the number of Ural blocking events that occurred (Fig. 1b). We found that only one UB event is seen in November prior to the 2016/17 winter. However, three UB events took place in the 2015/16 winter (Fig. 1b). Thus, it is possible that the difference in BKS sea ice variability between these two winters is due in part to the difference in the number of UB events.

Here, we further examine the large-scale circulation patterns associated with UB events during December 2015-February 2016 and December 2016-February 2017. We show the time-mean 500-hPa geopotential height and SAT anomalies averaged over the life cycles of the UB events for the 2015/16 and 2016/17 winters (Fig. 2). We found by examining the longitudinal movement of the UB events that the anomalously low BKS sea ice corresponds to two QUB events in the 2015/ 16 winter, and to one QUB event in November for the 2016/17 winter. For these blocking patterns, the QUB occurs together with a flow that projects onto the NAO⁺ (Figs. 2a,c,d), whereas the EUB coincides with a flow that projects onto NAO (Fig. 2b). As mentioned by B. Luo et al. (2017), the winter SIC increase is seen in the BKS when the UB occurs together with the NAO (their Fig. 2b), while the UB with the NAO⁺ favors the intrusion of midlatitude moisture into the BKS followed by a strong sea ice decline. In the 2015/16 winter the EUB-related SIC shows an increase because the water vapor in BKS is suppressed and the downward IR is reduced when the EUB occurs together with the NAO (Figs. 3b,e of B. Luo et al. 2017). On the other hand, because the EUB has a more eastward position and corresponds to a period of the negative SST anomaly in BKS (not shown), the role of the EUB in the SIC decline is also counteracted by the negative BKS SST anomaly. This is a major cause of why the EUB corresponds to a SIC increase (Fig. 1b). Such an effect becomes very different once the EUB occurs together with the NAO⁺ or it occurs without NAO (Figs. 2a,c of B. Luo et al. 2017). In fact, the EUB events are mostly related to the NAO⁺, as seen from our composite fields of EUB events below, and from our previous investigations (Luo et al. 2016b).

Because two QUB events occur during the period from December to February in the 2015/16 winter, they likely inhibit the winter sea ice growth resulting in negative SIC anomalies in the BKS (top of Fig. 1a). In contrast, for the 2016/17 winter, the winter sea ice is seen to increase from December to March (bottom of Fig. 1a) as the one QUB event occurs in November, whereas this blocking event may be linked to the low SIC state over BKS in November. Thus, it is speculated that the frequency of the UB and its zonal movement can make a

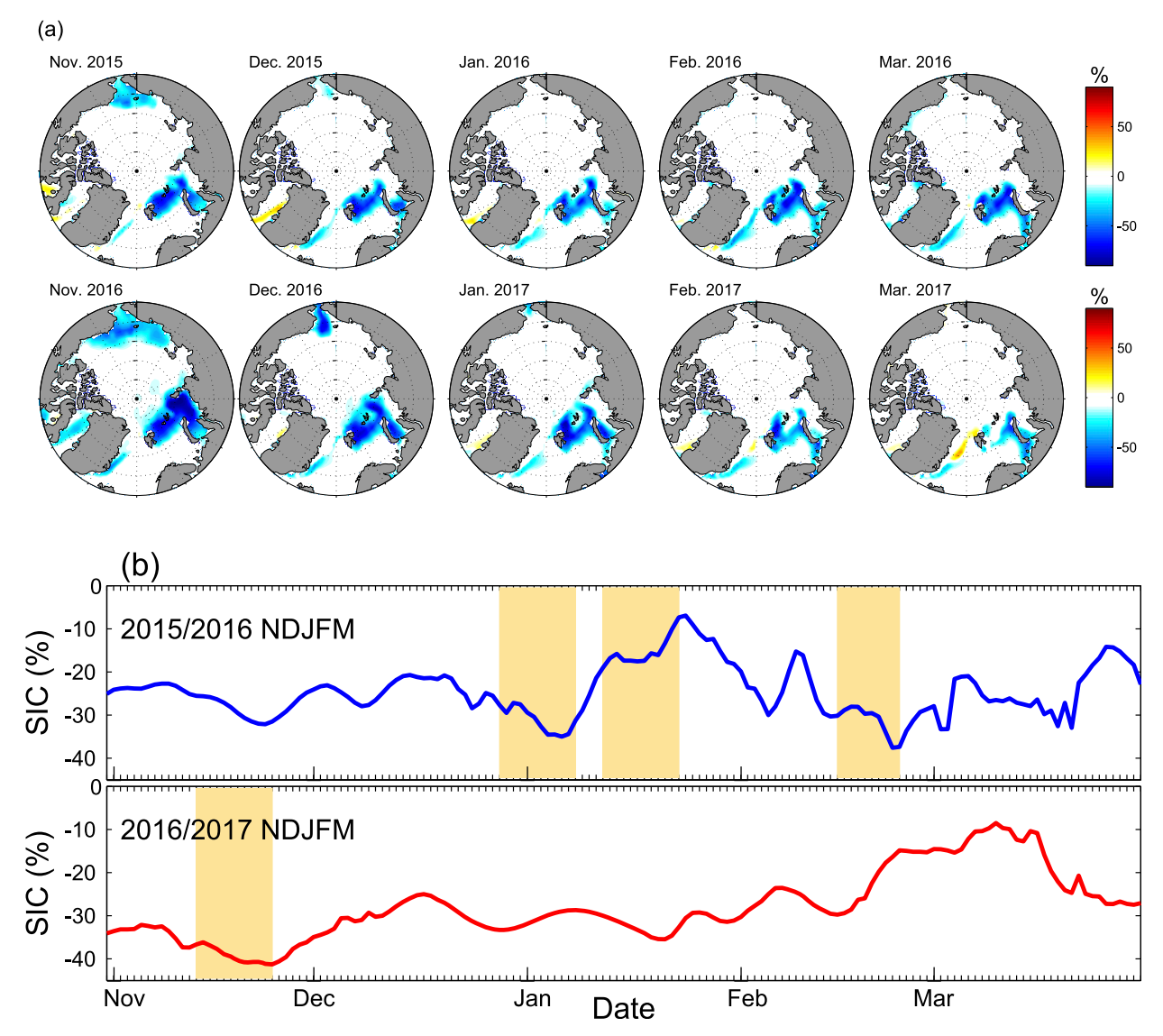


FIG. 1. (a) Monthly mean SIC anomaly patterns from November to March (NDJFM) in 2015/16 and 2016/17 winters and (b) the daily time series of their NDJFM SIC anomalies averaged over the BKS (65°–80°N, 30°–90°E). The yellow shading denotes the time interval of the UB occurrence.

significant contribution to the winter sea ice change in the BKS. In the following sections, we will examine if the movement of the UB has an important impact on the winter sea ice change in the BKS from winter-mean and daily perspectives.

4. Coupling between Arctic sea ice variability and the UB patterns

It is useful to first examine the time variation of the DJF-mean SIC over the BKS during 1979–2015 from monthly mean data. Here, we investigate if the decadal change in Arctic sea ice is related to the change in the

frequency of UB events with different zonal movements, even though our attention is placed on the short time variability of the Arctic sea ice. Our result shows that the 1979–88 SIC anomaly (deviation from the 1979–2015 average) averaged over the BKS is -1.83% decade $^{-1}$, whereas the 1989–98, 1999–2008, and 2009–15 anomalies are -1.09%, -9.0%, and -12.05% decade $^{-1}$, respectively (Fig. 3a). This indicates that the BKS sea ice undergoes a rapid decline after 1999. The decline rate per 10 years of BKS sea ice is statistically significant at the 95% confidence level based on a Student's t test. This result is also consistent with previous findings (Comiso 2006; Francis and Hunter 2007).

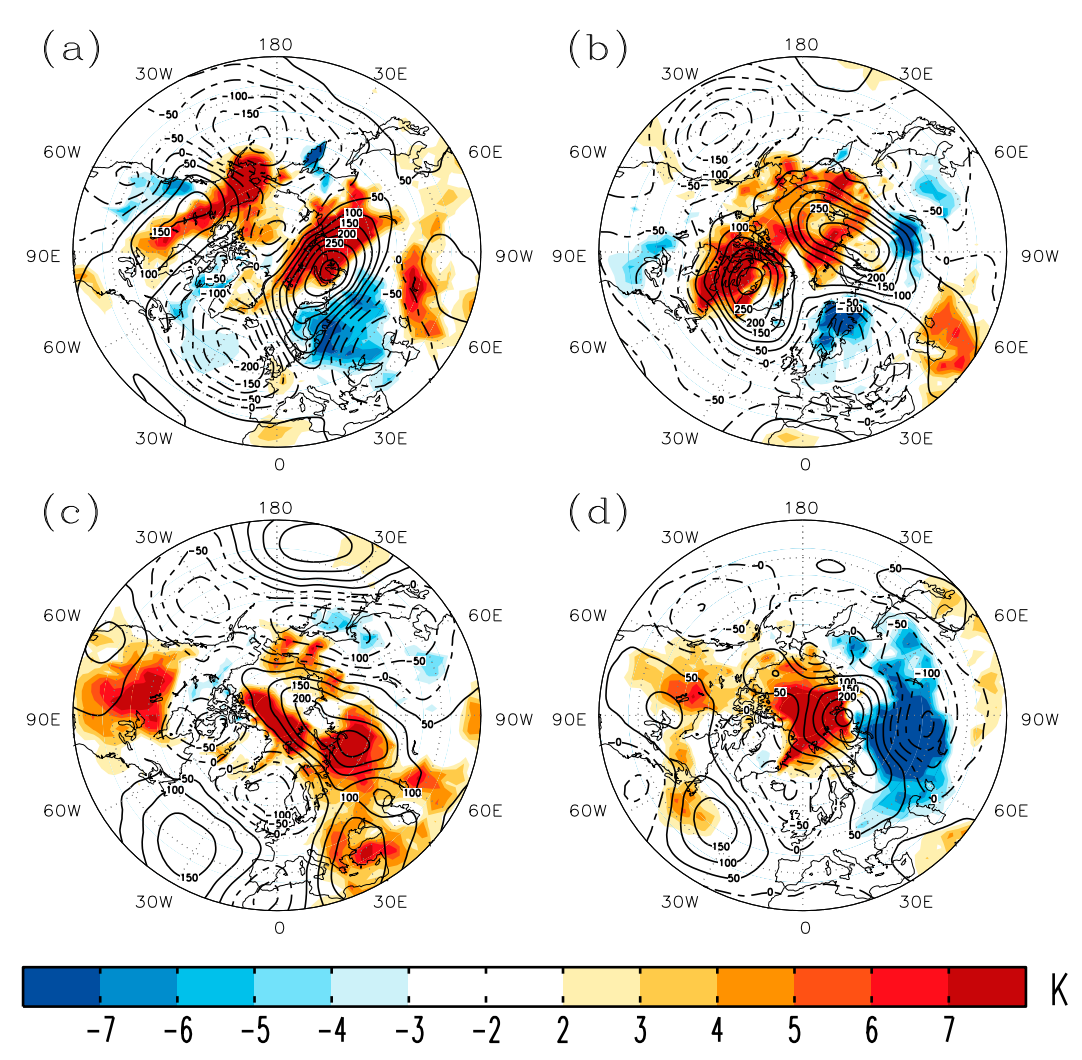


FIG. 2. Time-mean 500-hPa geopotential height (contour) and SAT (color shading) anomalies averaged over the life periods of UB events in the 2015/16 and 2016/17 winters: (a) 28 Dec 2015–7 Jan 2016, (b) 11–21 Jan 2016, (c) 15–23 Feb 2016, and (d) 14–24 Nov 2016.

The calculation shows for detrended SIC that there are three (1982, 1983, 1984) and six (2005, 2006, 2007, 2011, 2012, 2015) large negative winter SIC anomaly events (these events have SIC anomaly values that are less than -5%) during 1979–99 and 2000–15 (Fig. 3b). This indicates that large negative SIC anomaly events are more frequent during 2000-15 than during 1979-99. Figure 4 shows the interdecadal variation of QUB, WUB, and EUB events during 1979–2015. We can see that the frequency of WUB events exhibits a decreasing trend during 1979-2015, the frequency of QUB events increases significantly after 1999 relative to before, and the frequency of EUB events shows little change. In addition, the mean duration of the QUB, WUB, and EUB events during 1979–2015 is 7.31, 5.0, and 5.71 days respectively (not shown), indicating that the QUB is most persistent. Thus, it is plausible that the large decrease in SIC during 2000–15 is related to the increased frequency of QUB events. In this paper, we will focus our attention on examining the relationship between the short time scale variability of Arctic sea ice and the zonal movement of UB, because the decadal trend of the Arctic sea ice is related to frequency changes in QUB, WUB, and EUB events.

We further define a QUB, WUB, or EUB winter as corresponding to a winter when that particular pattern has the highest frequency. The calculation of the frequencies shows that there are 10 QUB (1983, 1984, 2000, 2007, 2008, 2009, 2010, 2011, 2012, 2015), 10 WUB (1979, 1980, 1985, 1987, 1990, 1995, 1996, 2001, 2002, 2003), and 6 EUB (1982, 1989, 1993, 1994, 2005, 2013) winters during 1979–2015. Thus, most of the large negative SIC

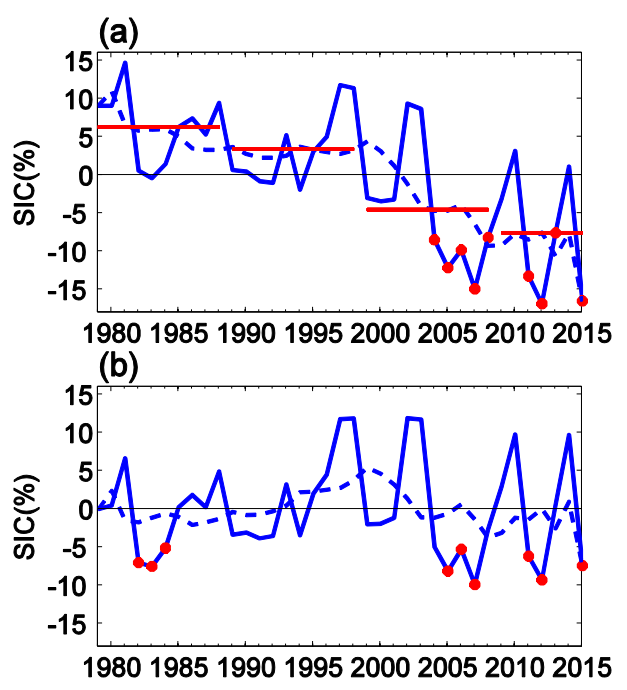


FIG. 3. Time series of (a) nondetrended and (b) detrended DJF-mean SIC anomalies over the BKS $(65^{\circ}-80^{\circ}N, 30^{\circ}-90^{\circ}E)$ during 1979–2015 for nonsmoothing (solid) and 9-yr smoothing (dashed) cases. The red dots denote the value of the winter SIC anomaly lower than -5%.

anomaly winters shown in Fig. 3b correspond to QUB events. We show the DJF-mean SIC anomalies for the three types of blocking cases in Fig. 5, which are plotted only for those areas above the 90% confidence level

based on a Monte Carlo test with a null hypothesis being an anomaly of zero. It can be seen that QUB and EUB winters correspond to reduced sea ice over the BKS (Figs. 5a,c), whereas a WUB winter shows an increase in sea ice (Fig. 5b). An interesting feature is that the sea ice shows opposite variation between the BKS and the Baffin Bay, Davis Strait, and Labrador Sea area (BDL) for WUB and EUB winters, likely because of the opposite zonal movement of the WUB and EUB. The result that the sea ice increases in BDL as UB moves eastward is easily explained because UB is often linked to the NAO⁺ (Luo et al. 2016b). The NAO⁺ upstream moves eastward as a part of the coupled NAO⁺ and UB system when the EUB moves eastward from Ural Mountains to Siberia and then leads to a strong widespread cooling in Greenland (Luo et al. 2016b). On the other hand, for the QUB events, the large loss of the Arctic sea ice over the BKS during the 1979-2015 time period is likely to be related to its greater persistence. To explore this possibility, we next examine the daily variation of UB events and the corresponding Arctic sea ice anomalies.

5. Impact of the UB movement on the sea ice change over the BKS

a. Movement characteristics of the UB patterns

As noted above, the different UB winters correspond to distinct DJF-mean SIC anomalies over the BKS, suggesting that each type of UB event has a different

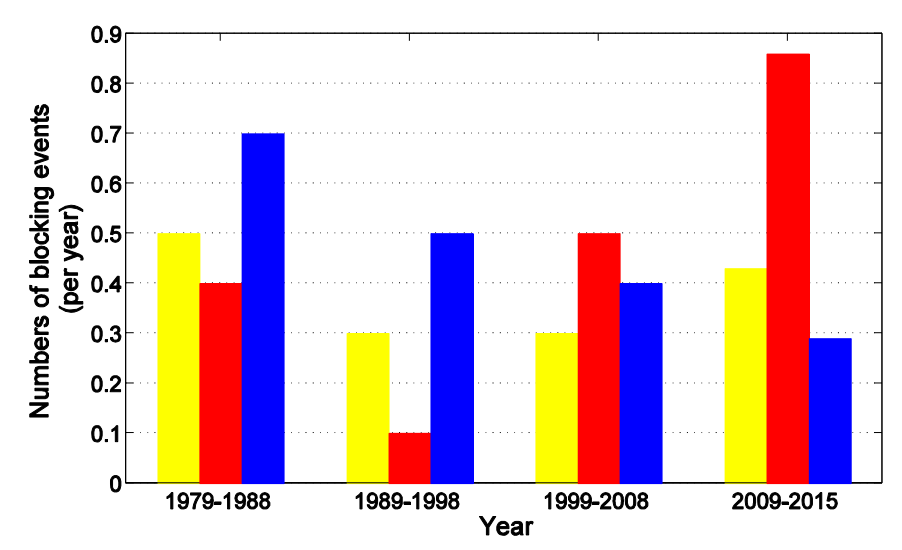


FIG. 4. Temporal variations of the numbers (frequency) of QUB (red), WUB (blue), and EUB (yellow) events per 10 year during 1979–2015 winters. The number in the ordinate denotes the mean number of events per year. The increased frequency of QUB events per year from 1989 to 2015 is statistically significant at the 95% confidence level based on a Student's *t* test, whereas the variation of WUB or EUB events during 1989–2015 is not statistically significant.

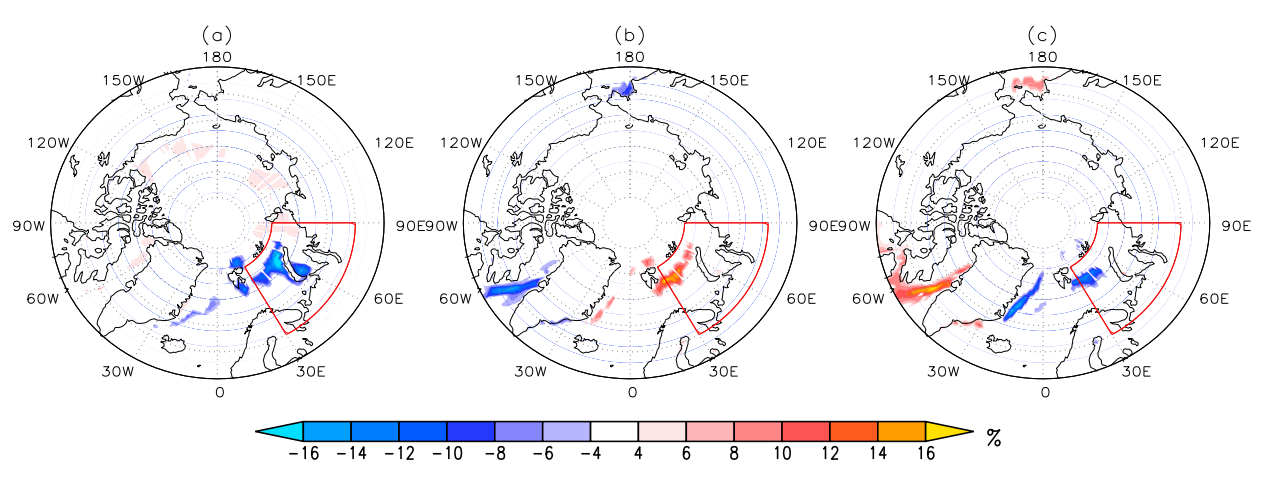


FIG. 5. Composite fields of DJF-mean SIC anomalies for (a) QUB (10 cases), (b) WUB (10 cases), and (c) EUB (6 cases) dominating winters from 1979 to 2015. The red (blue) shading denotes the positive (negative) anomaly area above the 90% confidence level for a Monte Carlo test. The red box denotes the Barents–Kara Sea (65°–80°N, 30°–90°E).

impact on Arctic sea ice variability over the BKS. To quantify these differences, we first examine the composite daily 500-hPa geopotential height anomaly fields (see Fig. 6) for QUB, WUB, and EUB events. As revealed in Fig. 6, all the three types of blocking events start to appear over the far northern end of the Ural Mountains, between 30° and 90°E, near the BKS. Because the QUB, as it is defined, is more persistent and quasi-stationary over the Ural region, it can generate a longer-lasting warming over the BKS (Fig. 6a). It is difficult for the WUB to show these persistence features because it undergoes retrogression (Fig. 6b). On the other hand, Fig. 6c shows that the anticyclonic anomaly of the EUB undergoes eastward movement. While the EUB has a smaller amplitude than the WUB, the EUB does show a warming, but the WUB shows a cooling over the BKS after lag +6 days (Fig. 6b), perhaps because the WUB moves westward to Greenland.

b. Relationship between the intraseasonal variability of Arctic sea ice and UB movement

To further explore the linkage of Arctic sea ice over the BKS with UB, it is useful to first look at the variations of composite daily SAT and SIC anomalies for the QUB, WUB, and EUB events. For the SAT, the domain is specified to be the region (65°–85°N, 30°–90°E), which is referred to as the BKS. But for the SIC, the region (65°–80°N, 30°–90°E) is chosen as the BKS, as this is the area where the large SIC decrease takes place. Because the SIC decline has a 4-day time lag behind the UB peak and persists for a rather long time even after the UB decays (Gong and Luo 2017), we show the time-mean SIC anomalies averaged from

 $\log -10$ to +30 days in Figs. 7a-c. It is interesting that the negative SIC anomaly in the BKS is largest for the QUB (Fig. 7a), weakest for the WUB (Fig. 7b), and intermediate for the EUB (Fig. 7c). Also, for the WUB, the SIC anomaly becomes positive in the BKS after lag 10 days, and the time mean from lag -10 to 40 days or longer is also positive (not shown). Figures 7d and 7e show the time series of the composite daily SAT and SIC anomalies averaged over the BKS for QUB (red line), WUB (blue line), and EUB (yellow line) events. We can see that before lag - 10 days the BKS-averaged SIC anomaly is negative for the QUB (Fig. 7d) and EUB (Fig. 7d) but positive for the WUB (Fig. 7d). This finding reflects the different precursor sea ice conditions for the QUB or EUB and WUB. It appears that the QUB and EUB require less prior SIC than the WUB. The SIC further decreases as the QUB or EUB begins to grow. The BKS SIC reaches a local minimum value at about lag +3 days and later at lag +16 days for the QUB, whereas its minimum peak is found at about lag +2 days for the EUB (Fig. 7d). Thus, there is a positive feedback between the SIC decline and QUB or EUB. The positive SAT anomaly is more intense and persistent in the BKS for the QUB (red line in Fig. 7e) than for the EUB (yellow line in Fig. 7e) even though the QUB amplitude decreases more rapidly after lag 0. This more intense and persistent positive SAT anomaly in BKS for the QUB can lead to a more persistent negative SIC anomaly compared to the EUB. Our calculation shows that the difference of the BKSaveraged SIC (SAT) anomaly time series between the QUB and EUB during the blocking decay and disappearance phases is statistically significant at the 90% confidence level for a Monte Carlo test with 5000

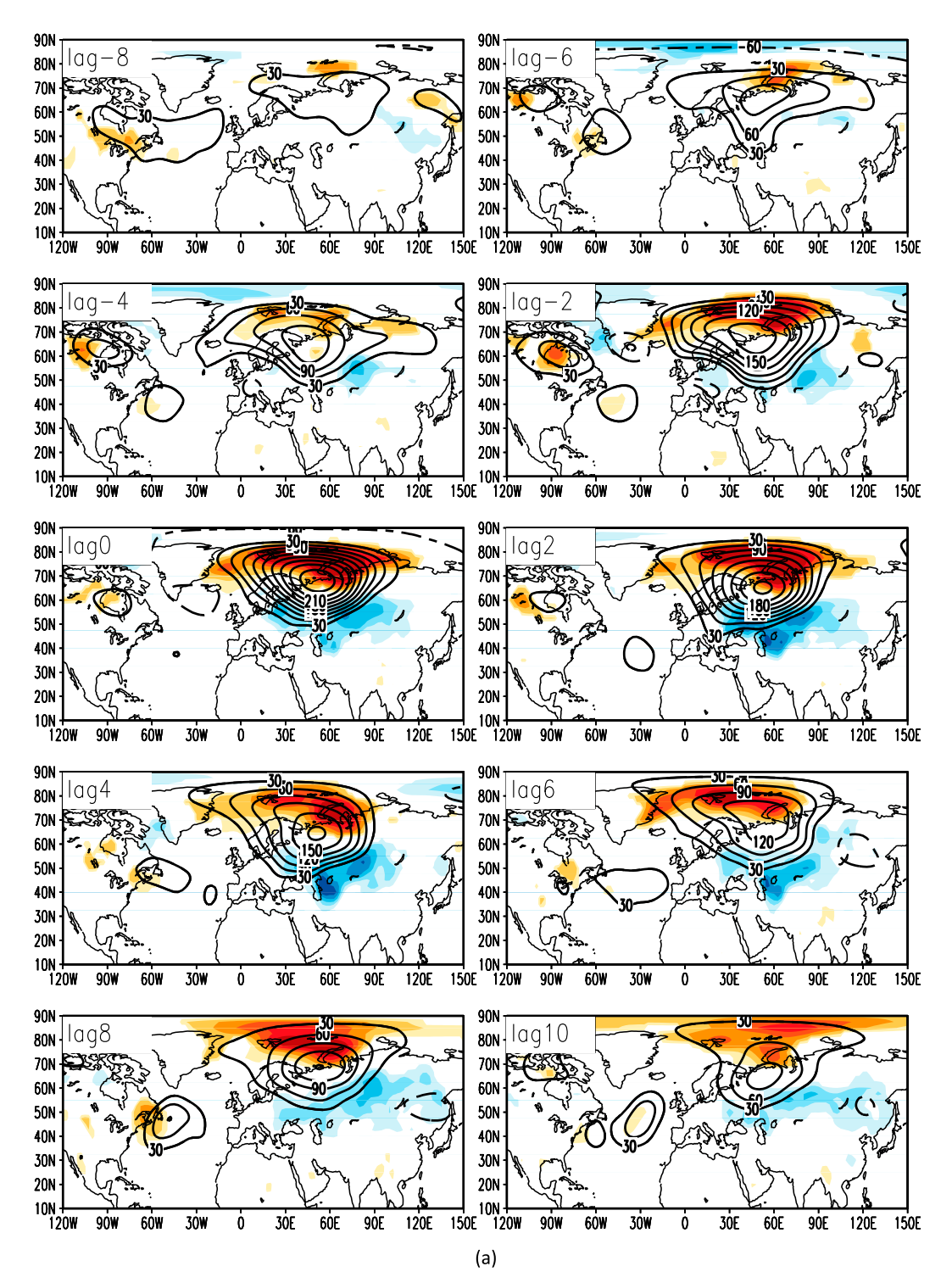


FIG. 6. Instantaneous horizontal fields of composite daily 500-hPa geopotential height (contour; unit: gpm) and SAT (shading; unit: K) anomalies for (a) QUB (16 cases), (b) WUB (18 cases), and (c) EUB (14 cases) events during 1979–2015. The red (blue) shading and contours denote the positive (negative) anomaly areas above the 90% confidence level based on a two-sided Student's *t* test. Lag 0 denotes the peak day of the UB event.

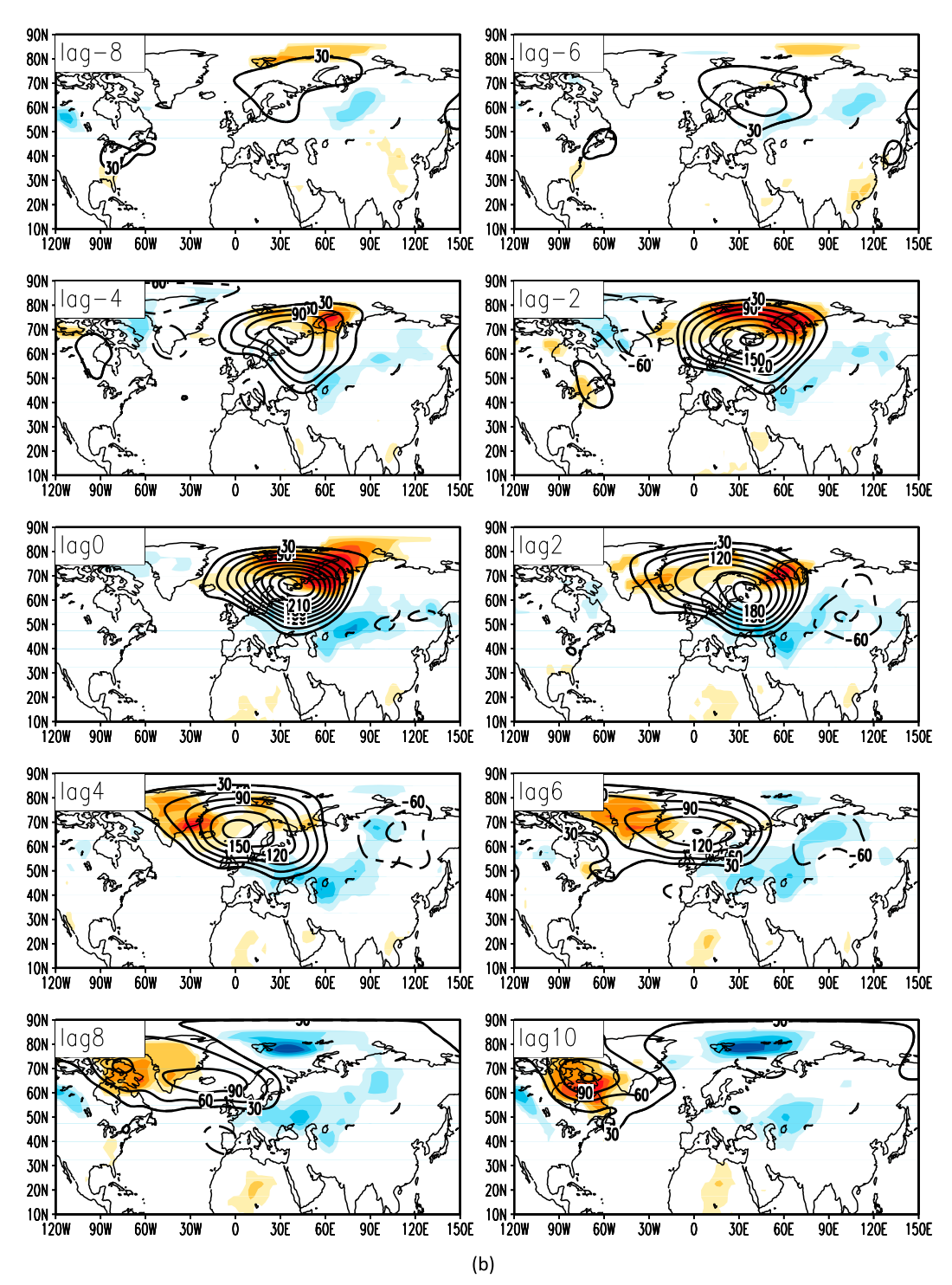


FIG. 6. (Continued)

random simulations. The growth of the WUB also coincides with a decline in the BKS SIC anomaly, but the reduction in sea ice does not persist as long as that for the QUB and EUB events. Instead, the WUB BKS-averaged SIC anomaly becomes positive after lag +10 days and the

corresponding SAT anomaly becomes negative after lag +6 days (blue line in Fig. 7e). The Monte Carlo test also shows that the difference of the SIC (SAT) between the QUB and WUB is statistically significant at the 90% confidence level. This indicates that the QUB, EUB, and

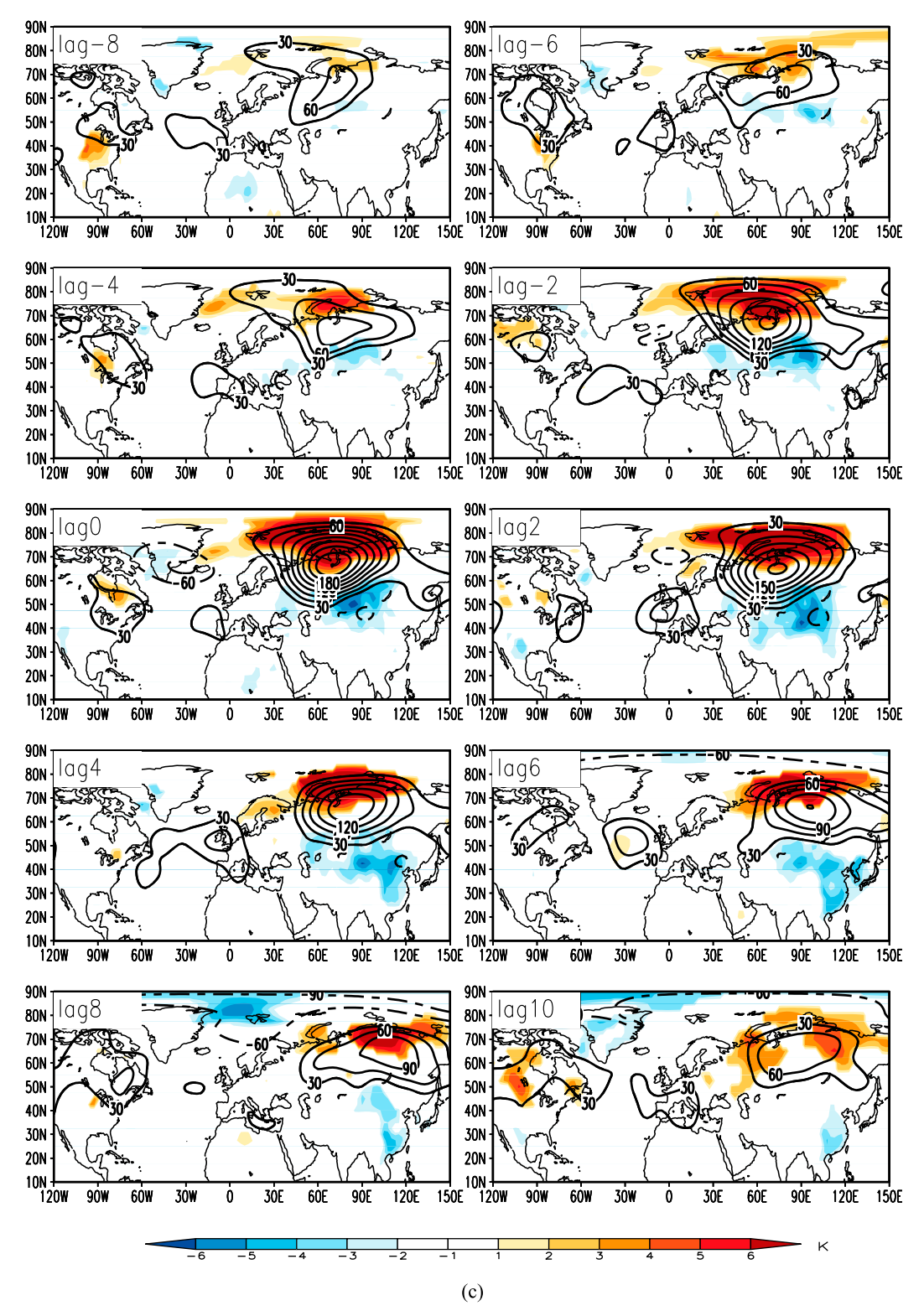


FIG. 6. (Continued)

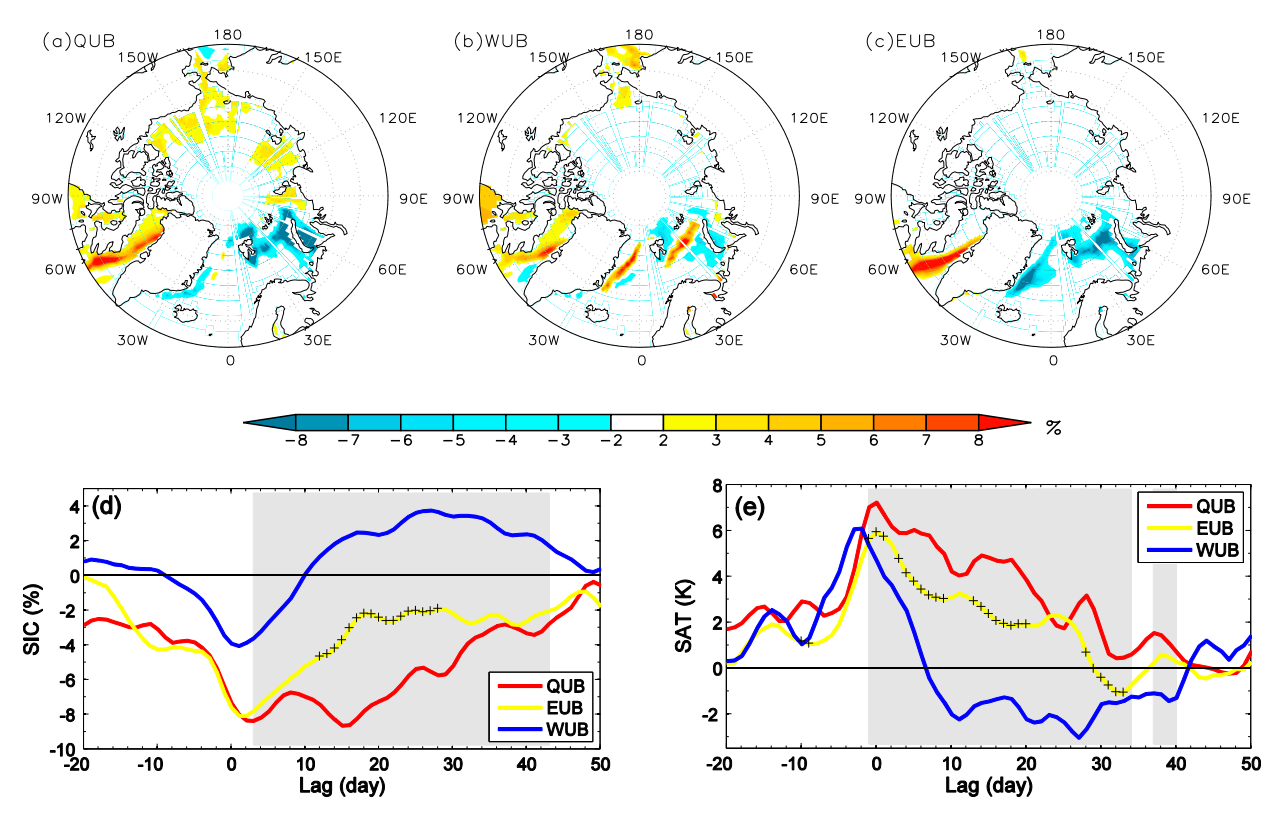


FIG. 7. Time-mean fields of SIC anomalies during the blocking life cycle averaged from lag -10 to 30 days for the (a) QUB, (b) WUB, and (c) EUB. Also shown are time series of latitude-weighted domain-averaged composite daily detrended (d) SIC anomalies in the BKS region (65°–80°N, 30°–90°E) and (e) SAT anomalies in the BKS (65°–85°N, 30°–90°E) where the land has been excluded for a domain average) for QUB (red), WUB (blue), and EUB (yellow) events during 1979–2015. In (a)–(c), the color shading denotes the region above the 90% confidence level for a two-sided Student's t test and lag 0 denotes the peak day of the UB. The gray shading denotes the lags where the difference of the SAT (Fig. 5d) or SIC (Fig. 5e) time series between the QUB and WUB is significant at the 90% confidence level based on a Monte Carlo test. The cross represents their difference between the QUB and EUB being significant at a 90% confidence level. The latitude weighting of the variable α at each grid point in the latitude band from the south latitude ϕ_{PS} to the north latitude ϕ_{PN} represents $\alpha \cos \phi/\cos(\phi_M)$, where $\phi_M = (\phi_{PS} + \phi_{PN})/2$ and $\phi_{PS} \le \phi \le \phi_{PN}$.

WUB have different and important impacts on the SIC change over the BKS.

c. Downward infrared radiation and sensible and latent heat fluxes that drive the intraseasonal sea ice variability

While previous studies indicated that the direction and strength of the winds in the Arctic play a role in sea ice decline due to sea ice drift (Jung and Hilmer 2001), here we will demonstrate that the downward IR associated with the UB pattern appears to play an important role in the SIC decrease. This can be crudely seen from the direction of horizontal surface winds during the UB life cycle. We show the time-mean surface (10 m) wind anomaly vector fields for the QUB, WUB, and EUB patterns averaged from lag -10 to 0 days and lag 0 to 10 days in Fig. 8. It can be seen that the surface westerly or southerly wind anomalies are dominant in the BKS north of 70°N when the QUB, WUB, or EUB pattern

occurs. This implies that the surface wind anomaly distributions associated with QUB, WUB, and EUB patterns (Fig. 8) are not favorable for the sea ice drift out of the BKS. But southwesterly winds can push the sea ice edge northward to result in a decrease in the sea ice extent. Perhaps along with the surface winds pushing the sea ice northward during these UB events the IR is also playing a role as well. Thus, below we will only examine the role of surface energy fluxes and downward IR in the sea ice change.

Downward IR at the surface has been identified as the dominant contributor to winter intraseasonal SIC variability (D.-S. R. Park et al. 2015). Furthermore, the importance of downward IR for winter Arctic warming has been shown in a growing body of literature (Doyle et al. 2011; Lee et al. 2011; Lesins et al. 2012; Yoo et al. 2012a,b; Woods et al. 2013; Liu and Key 2014; H.-S. Park et al. 2015; Woods and Caballero 2016; Letterly et al. 2016; Gong and Luo 2017; Gong et al. 2017; Lee et al. 2017). This is at odds with the theory that surface heat

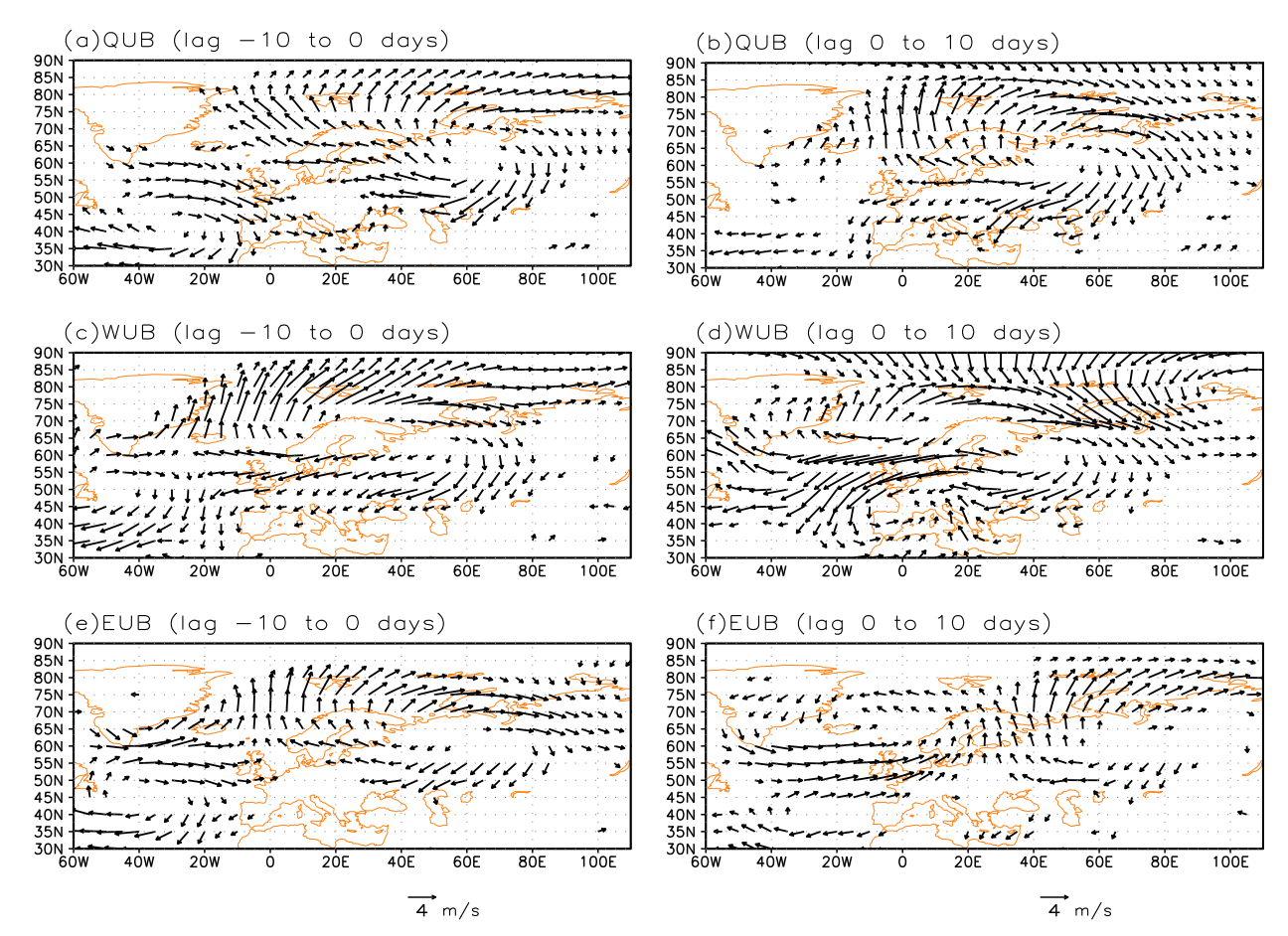
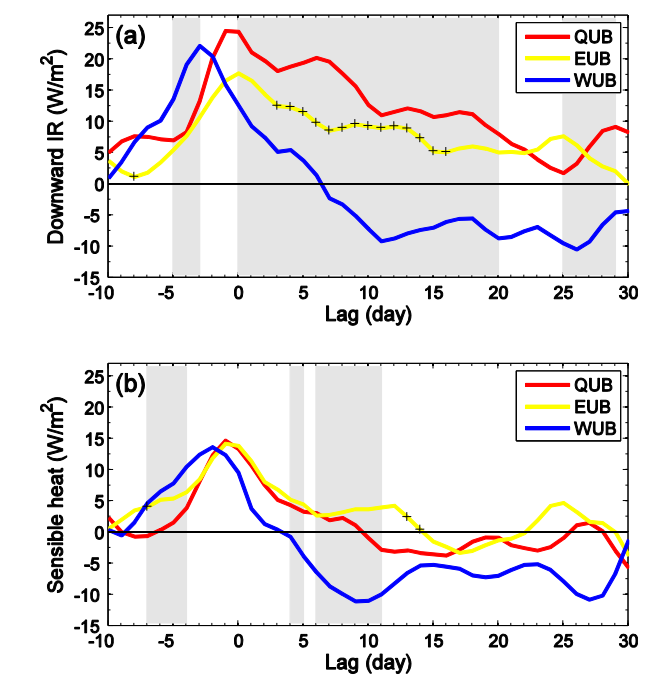


FIG. 8. Time-mean vector fields of composite daily horizontal winds averaged over the time periods (left) from lag -10 to 0 days and (right) lag 0 to 10 days for (a),(b) QUB, (c),(d) WUB, and (e),(f) EUB events. The arrow denotes the wind direction and the region of the wind vector larger than 3 m s⁻¹ is only plotted in these figures.

flux plays the dominant role (e.g., Serreze and Francis 2006; Screen and Simmonds 2010b; Stroeve et al. 2012). Thus, to help understand how UB can lead to the variability of Arctic sea ice, we calculate the time series of BKS-averaged downward IR, downward sensible heat flux (SHF), and latent heat flux (LHF) anomalies in Fig. 9 for the QUB, WUB, and EUB (in the BKS the land and marginal regions with the SIC less than 50% have been excluded in calculating an area average). The statistical significance of the difference between the QUB and WUB time series and also the QUB and EUB time series in Fig. 9 is tested using a Monte Carlo method with 5000 random simulations. It is found from Fig. 9 that the difference of the BKS-averaged downward IR between the QUB and WUB and also the QUB and EUB is statistically significant during the blocking decay and disappearance phases.

It is further seen that while the downward IR anomaly is positive over the BKS throughout the lag -10 to lag 30 days time period (Fig. 9a) for the QUB and EUB, it is

much stronger for the QUB. The intense and persistent positive downward IR is closely related to increased water vapor in the BKS (Gong and Luo 2017; B. Luo et al. 2017). Thus, for the QUB, the intense and persistent downward IR anomaly can lead to a notable long-lasting BKS warming as seen in Fig. 9a (red line), while the SHF also has a large contribution to the BKS warming during the mature period (from lag -5 to 5 days; Fig. 9b). Consequently, the QUB is able to lead to a large decline of the BKS ice. For the EUB, the contributions of downward IR and SHF anomalies to the BKS ice decline are comparable during the blocking mature phase. In fact, the SHF is about half the value of the downward IR after lag +3, thus implying that the downward IR is still dominant. This result is basically consistent with the finding of D.-S. R. Park et al. (2015), who emphasized that the downward IR plays the dominant role. An interesting result is found that whereas the SHF and LHF anomalies remain close to zero after lag +5 days for the QUB and EUB, the downward IR persists for a longer



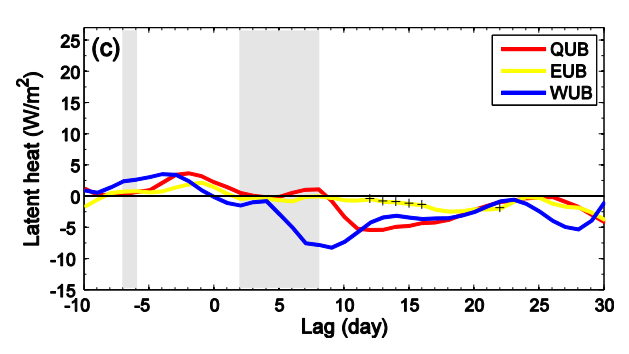


FIG. 9. Time series of latitude-weighted and domain-averaged composite daily surface (a) downward infrared radiation (IR) anomalies, (b) downward sensible heat (SHF), and (c) latent heat flux (LHF) anomalies in the region (65°–85°N, 30°–90°E, where the land and marginal regions with the SIC less than 50% have been excluded for a domain average) for QUB (red), WUB (blue), and EUB (yellow) events. The gray shading denotes the lags where the difference of the downward IR, SHF, and LHF between the QUB and WUB is significant at the 90% confidence level based on a Monte Carlo test. The cross denotes their difference between the QUB and EUB being significant.

time until lag +25 days. For the WUB, the downward IR and SHF anomalies contribute to the BKS warming during its growth and mature phases (from lag -10 to 5 days; Figs. 9a,b). But during the disappearance phase (after about lag +5 days) of the WUB the downward IR, SHF, and LHF anomalies become negative and have comparable contributions to the BKS cooling as seen in Fig. 9b (blue line). This BKS cooling leads to a large rise of the BKS ice during the disappearance phase of the WUB (blue line in Fig. 7d). Thus, the above results indicate that a SHF cannot account for the persistent SIC

decrease and SAT increase in the BKS (Figs. 7d,e). Rather, downward IR is the main driver of the sea ice loss for the QUB and EUB, while the SHF is also important.

It is useful to calculate the time mean of these quantities from lag -5 to 5 days (lag 0 denotes the peak day of the blocking) to estimate their relative contributions to the Arctic warming over the BKS during the mature phase of blocking. We show the time-mean BKSaveraged surface downward IR, SHF, and LHF anomalies over the mature period (from lag - 5 to 5 days) in Fig. 10a for the OUB, WUB, and EUB events. It is noted that during the blocking mature phase the time-mean downward IR anomaly is 2.4 (2.9) times larger than the downward SHF for the QUB (EUB) events, which plays a larger role in the BKS warming than the SHF for the QUB (left) and EUB (right) (blue shading in Fig. 10a). For the WUB, the time-mean downward IR is 1.8 times greater than the time-mean SHF anomaly during the WUB mature period (middle column in Fig. 10a). Also, averaged over the entire life cycle (from lag -10 to 10 days) of QUB events (Fig. 10b), we see that the downward SHF is stronger for the EUB than for the QUB. The downward IR appears to play a more important role in the BKS warming than the SHF because the time-mean downward IR anomaly is 3.3 times larger than the time-mean SHF anomaly. However, for the EUB, the downward IR and SHF play comparable roles in the BKS warming in that the time-mean downward IR anomaly is 1.55 times greater than the time-mean SHF anomaly. It is also found that the LHF plays a minor role in the BKS warming for the QUB, WUB, and EUB (Fig. 10).

Although the downward IR anomaly is more important for the BKS warming than the SHF during the mature duration of the QUB, WUB, and EUB (Fig. 10a), the SHF anomaly becomes negative during the blocking disappearance phase of the WUB (Figs. 9b,c) resulting in the timemean SHF anomaly being slightly negative. This is clearly seen from a long time mean (from lag -10 to 20 days or $\log -10$ to 30 days) (not shown). Thus, over the entire life cycle (from lag -10 to 10 days) of WUB events, the net contribution of WUB to the BKS sea ice decline is relatively weak for the downward IR and SHF anomalies respectively, and even negative for the LHF anomalies. This result also holds for the life time of the anomaly (e.g., from lag -10 to 30 days; not shown). It is worth reiterating here that during the blocking mature period, and over its entire life cycle, the SHF warming for all three UB cases is from the atmosphere, not the ocean.

6. Conclusions and discussion

In this paper, we first performed a case study of the BKS sea ice variation for two recent winters, 2015/16 and 2016/

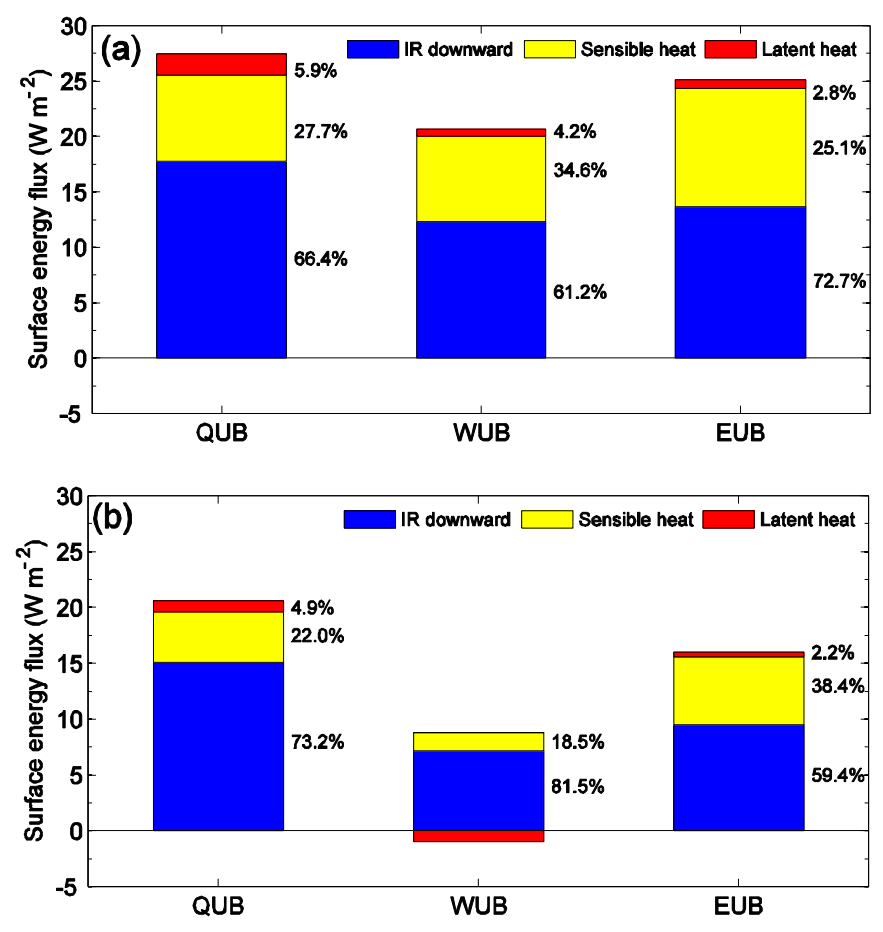


FIG. 10. Latitude-weighted and area-averaged surface energy flux over the region $(65^\circ-85^\circ N, 30^\circ-90^\circ E)$ where lands and marginal region with the SIC less than 50% have been excluded for a domain average) averaged over time intervals from (a) lag -5 to 5 days (mature period) and (b) lag -10 to 10 days (life cycle). The blue box denotes the surface downward IR, the yellow box denotes the downward surface sensible heat flux, and the red box denote the downward surface latent heat flux. The number in the right side of each box denotes the percentage of its each component (>0) with respect to the total surface energy flux. The calculation of the percentage does not consider the negative latent heat anomaly in Fig. 10b.

17, and found that the winter sea ice change in the BKS is closely related to the occurrence of UB events. Then we analyzed the long-term variation of winter Ural blocking (UB) events during 1979–2015 by classifying the UB events into three categories: quasi-stationary (QUB) and eastward- (EUB) and westward-shifting (WUB) UB patterns. It is shown that whereas the WUB frequency undergoes a decreasing trend from 1979 to 2015, and the EUB shows little trend over this time period, the QUB frequency shows a significant upward trend during 1999–2015.

The daily data analysis here demonstrates that the QUB appears to play a more important role in the BKS sea ice decline compared to the EUB and WUB because it is associated with more intense and persistent warming over the BKS (red line in Fig. 7a) due to stronger downward IR related to more abundant water vapor in

the BKS (Gong and Luo 2017). The intense and persistent warming related to the QUB is able to lead to a large SIC decline in the BKS although the QUB requires lesser SIC extent, and the peak of the sea ice decline lags the blocking peak by about 3 days. Thus, there is a positive feedback between the SIC decline and QUB. This may explain in part why there is a rapid decline of the winter BKS sea ice during 1999-2015. Our calculations also reveal that downward IR plays the main role in driving sea ice decline for the QUB, whereas downward IR and sensible heat flux have comparable contributions to the SIC variation for the WUB and EUB. The WUB has different contributions to the BKS SIC variation during its growth and decay phases. During the blocking growth phase downward sensible heat flux has a comparable magnitude with that of downward IR

for the WUB, resulting in a decline in sea ice. But during the blocking decay phase, downward IR and sensible heat flux becomes persistently negative (Fig. 9a), which leads to a steady BKS SIC rise.

Given the above finding, a natural question to ask is why the frequency of the QUB events has increased. Because the UB often is linked to the presence of an NAO⁺ (Luo et al. 2016b), it is possible that the decadal change in the QUB events (the lack of zonal movement) is modulated by the decadal NAO variability. Because NAO variability on decadal and multidecadal time scales is related to North Atlantic SST warming and the phase of the Atlantic multidecadal oscillation (AMO) (Peings and Magnusdottir 2014), it is possible that the AMO is modulating the stationarity of the UB pattern. This AMO-atmosphere-sea ice mechanism is different from the previously suggested mechanism of a warmer ocean water having a direct impact on the sea ice (Mahajan et al. 2011; Day et al. 2012; Miles et al. 2014). In the future, we will explore the AMO-atmospheresea ice mechanism and the influence of North Atlantic SST on the UB.

Acknowledgments. The authors acknowledge the support from the Chinese Academy of Sciences Strategic Priority Research Program (Grant XDA19070403), the National Natural Science Foundation of China (41790473, 41430533), and U.S. National Science Foundation Grants AGS-1455577, AGS-1401220, and OPP-1723832. This paper was written as the second author was a visiting scientist at the Department of Meteorology and Atmospheric Science, The Pennsylvania State University, during his stay from September to October 2016. The authors would like to thank three anonymous reviewers for their useful suggestions, which helped improve the quality of this paper.

REFERENCES

- Baggett, C., S. Lee, and S. B. Feldstein, 2016: An investigation of the presence of atmospheric rivers over the North Pacific during planetary-scale wave life cycles and their role in Arctic warming. J. Atmos. Sci., 73, 4329–4347, https://doi.org/10.1175/ JAS-D-16-0033.1.
- Boisvert, L. N., A. A. Petty, and J. C. Stroeve, 2016: The impact of the extreme winter 2015/16 Arctic cyclone on the Barents– Kara Seas. Mon. Wea. Rev., 144, 4279–4287, https://doi.org/ 10.1175/MWR-D-16-0234.1.
- Cohen, J., and Coauthors, 2014: Recent Arctic amplification and extreme mid-latitude weather. *Nat. Geosci.*, 7, 627–637, https://doi.org/10.1038/ngeo2234.
- Comiso, J. C., 2006: Abrupt decline in the Arctic winter sea ice cover. Geophys. Res. Lett., 33, L18504, https://doi.org/10.1029/ 2006GL027341.
- Day, J. J., J. C. Hargreaves, J. D. Annan, and A. Abe-Ouchi, 2012: Source of multi-decadal variability in Arctic sea ice extent.

- Environ. Res. Lett., 7, 034011, https://doi.org/10.1088/1748-9326/7/3/034011.
- Dee, D. P., and Coauthors, 2011: The ERA-Interim reanalysis: Configuration and performance of the data assimilation system. *Quart. J. Roy. Meteor. Soc.*, **137**, 553–597, https://doi.org/10.1002/qi.828.
- Doyle, J. G., G. Lesins, C. P. Thackray, C. Perro, G. J. Nott, T. J. Duck, R. Damoah, and J. R. Drummond, 2011: Water vapor intrusions into the high Arctic during winter. *Geophys. Res. Lett.*, 38, L12806, https://doi.org/10.1029/2011GL047493.
- Fang, Z., and J. M. Wallace, 1994: Arctic sea ice variability on a timescale of weeks and its relation to atmospheric forcing. *J. Climate*, 7, 1897–1914, https://doi.org/10.1175/1520-0442 (1994)007<1897:ASIVOA>2.0.CO;2.
- Forbes, B. C., and Coauthors, 2016: Sea ice, rain-on-snow and tundra reindeer nomadism in Arctic Russia. *Biol. Lett.*, **12**, 20160466, https://doi.org/10.1098/rsbl.2016.0466.
- Francis, J. A., and E. Hunter, 2007: Drivers of declining sea ice in the Arctic winter: A tale of two seas. *Geophys. Res. Lett.*, **34**, L17503, https://doi.org/10.1029/2007GL030995.
- Ghatak, D., and J. Miller, 2013: Implications for Arctic amplification of changes in the strength of the water vapor feedback. J. Geophys. Res. Atmos., 118, 7569–7578, https://doi.org/10.1002/jgrd.50578.
- Gong, T., and D. Luo, 2017: Ural blocking as an amplifier of the Arctic sea ice decline in winter. J. Climate, 30, 2639–2654, https://doi.org/10.1175/JCLI-D-16-0548.1.
- ——, S. Feldstein, and S. Lee, 2017: The role of downward infrared radiation in the recent Arctic winter warming trend. *J. Climate*, 30, 4937–4949, https://doi.org/10.1175/JCLI-D-16-0180.1.
- Jung, T., and M. Hilmer, 2001: The link between the North Atlantic Oscillation and Arctic sea ice export through Fram Strait. J. Climate, 14, 3932–3943, https://doi.org/10.1175/1520-0442(2001)014<3932: TLBTNA>2.0.CO:2.
- Kalnay, E., and Coauthors, 1996: The NCEP/NCAR 40-Year Reanalysis Project. *Bull. Amer. Meteor. Soc.*, 77, 437–471, https://doi.org/10.1175/1520-0477(1996)077<0437:TNYRP>2.0.CO;2.
- Lee, S., T. Gong, N. C. Johnson, S. B. Feldstein, and D. Pollard, 2011: On the possible link between tropical convection and the Northern Hemisphere Arctic surface air temperature change between 1958 and 2001. J. Climate, 24, 4350–4367, https://doi.org/ 10.1175/2011JCLI4003.1.
- —, —, S. B. Feldstein, J. A. Screen, and I. Simmonds, 2017: Revisiting the cause of the 1989–2009 Arctic surface warming using the surface energy budget: Downward infrared radiation dominates the surface fluxes. *Geophys. Res. Lett.*, 44, 10654– 10661, https://doi.org/10.1002/2017GL075375.
- Lesins, G., T. J. Duck, and J. R. Drummond, 2012: Surface energy balance framework for Arctic amplification of climate change. J. Climate, 25, 8277–8288, https://doi.org/10.1175/JCLI-D-11-00711.1.
- Letterly, A., J. Key, and Y. Liu, 2016: The influence of winter cloud on summer sea ice in the Arctic, 1983–2013. *J. Geophys. Res. Atmos.*, **121**, 2178–2187, https://doi.org/10.1002/2015JD024316.
- Liu, Y., and J. R. Key, 2014: Less winter cloud aids summer 2013 Arctic sea ice return from 2012 minimum. *Environ. Res. Lett.*, 9, 044002, https://doi.org/10.1088/1748-9326/9/4/044002.
- Luo, B., D. Luo, L. Wu, L. Zhong, and I. Simmonds, 2017: At-mospheric circulation patterns which promote winter Arctic sea ice decline. *Environ. Res. Lett.*, 12, 054017, https://doi.org/10.1088/1748-9326/aa69d0.
- Luo, D., Y. Xiao, Y. Yao, A. Dai, I. Simmonds, and C. L. E. Franzke, 2016a: Impact of Ural blocking on winter warm Arctic-cold Eurasian anomalies. Part I: Blocking-induced amplification. *J. Climate*, 29, 3925–3947, https://doi.org/10.1175/JCLI-D-15-0611.1.

- —, Y. Diao, A. Dai, C. L. E. Franzke, and I. Simmonds, 2016b: Impact of Ural blocking on winter warm Arctic-cold Eurasian anomalies. Part II: The link to the North Atlantic Oscillation. *J. Climate*, **29**, 3949–3971, https://doi.org/10.1175/JCLI-D-15-0612.1.
- —, Y. Yao, A. Dai, I. Simmonds, and L. Zhong, 2017: Increased quasi stationarity and persistence of winter Ural blocking and Eurasian extreme cold events in response to Arctic warming. Part II: A theoretical explanation. *J. Climate*, 30, 3569–3587, https://doi.org/10.1175/JCLI-D-16-0262.1.
- Mahajan, S., R. Zhang, and T. L. Delworth, 2011: Impact of the Atlantic meridional overturning circulation (AMOC) on Arctic surface air temperature and sea ice variability. *J. Climate*, 24, 6573–6581, https://doi.org/10.1175/2011JCLI4002.1.
- Miles, M. W., D. V. Divine, T. Furevik, E. Jansen, M. Moros, and A. E. J. Ogilvie, 2014: A signal of persistent Atlantic multidecadal variability in Arctic sea ice. *Geophys. Res. Lett.*, 41, 463–469, https://doi.org/10.1002/2013GL058084.
- Mori, M., M. Watanabe, H. Shiogama, J. Inoue, and M. Kimoto, 2014: Robust Arctic sea-ice influence on the frequent Eurasian cold winters in past decades. *Nat. Geosci.*, 7, 869–873, https:// doi.org/10.1038/ngeo2277.
- Overland, J., K. R. Wood, and M. Wang, 2011: Warm Arctic—cold continents: Climate impacts of the newly open Arctic Sea. *Polar Res.*, 30, 15787, https://doi.org/10.3402/polar.v30i0.15787.
- —, J. A. Francis, R. Hall, E. Hanna, S.-J. Kim, and T. Vihma, 2015: The melting Arctic and midlatitude weather patterns: Are they connected? *J. Climate*, 28, 7917–7932, https://doi.org/ 10.1175/JCLI-D-14-00822.1.
- Park, D.-S. R., S. Lee, and S. B. Feldstein, 2015: Attribution of the recent winter sea ice decline over the Atlantic sector of the Arctic Ocean. *J. Climate*, 28, 4027–4033, https://doi.org/ 10.1175/JCLI-D-15-0042.1.
- Park, H.-S., S. Lee, S.-W. Son, S. B. Feldstein, and Y. Kosaka, 2015: The impact of poleward moisture and sensible heat flux on Arctic winter sea ice variability. *J. Climate*, 28, 5030–5040, https://doi.org/10.1175/JCLI-D-15-0074.1.
- Peings, Y., and G. Magnusdottir, 2014: Forcing of the wintertime atmospheric circulation by the multidecadal fluctuations of the North Atlantic Ocean. *Environ. Res. Lett.*, 9, 034018, https://doi.org/10.1088/1748-9326/9/3/034018.
- Screen, J. A., and I. Simmonds, 2010a: Increasing fall-winter energy loss from the Arctic Ocean and its role in Arctic temperature amplification. *Geophys. Res. Lett.*, 37, L16707, https://doi.org/10.1029/2010GL044136.
- —, and —, 2010b: The central role of diminishing sea ice in recent Arctic temperature amplification. *Nature*, **464**, 1334– 1337, https://doi.org/10.1038/nature09051.
- —, and —, 2013a: Exploring links between Arctic amplification and mid-latitude weather. *Geophys. Res. Lett.*, **40**, 959–964, https://doi.org/10.1002/grl.50174.

- —, and —, 2013b: Caution needed when linking weather extremes to amplified planetary waves. *Proc. Natl. Acad. Sci. USA*, **110**, E2327, https://doi.org/10.1073/pnas.1304867110.
- Serreze, M. C., and J. A. Francis, 2006: The Arctic amplification debate. Climatic Change, 76, 241–264, https://doi.org/10.1007/ s10584-005-9017-y.
- Shimada, K., T. Kamoshida, M. Itoh, S. Nishino, E. Carmack, F. McLaughlin, S. Zimmermann, and A. Proshutinsky, 2006: Pacific Ocean inflow: Influence on catastrophic reduction of sea ice cover in the Arctic Ocean. *Geophys. Res. Lett.*, 33, L08605, https://doi.org/10.1029/2005GL025624.
- Simmonds, I., 2015: Comparing and contrasting the behaviour of Arctic and Antarctic sea ice over the 35 year period 1979–2013. *Ann. Glaciol.*, **56**, 18–28, https://doi.org/10.3189/2015AoG69A909.
- Spielhagen, R. F., and Coauthors, 2011: Enhanced modern heat transfer to the Arctic by warm Atlantic water. *Science*, 331, 450–453, https://doi.org/10.1126/science.1197397.
- Stroeve, J. C., M. C. Serreze, M. M. Holland, J. E. Kay, J. Malanik, and A. P. Barrett, 2012: The Arctic's rapidly shrinking sea ice cover: A research synthesis. *Climatic Change*, 110, 1005–1027, https://doi.org/10.1007/s10584-011-0101-1.
- Tibaldi, S., and F. Molteni, 1990: On the operational predictability of blocking. *Tellus*, 42A, 343–365, https://doi.org/10.3402/ tellusa.y42i3.11882.
- Von Storch, H., and F. W. Zwiers, 2001: Statistical Analysis in Climate. Cambridge University Press, 494 pp.
- Walsh, J. E., 2014: Intensified warming of the Arctic: Causes and impacts on middle latitudes. *Global Planet. Change*, **117**, 52– 63, https://doi.org/10.1016/j.gloplacha.2014.03.003.
- Wilks, D. S., 2011: Statistical Methods in the Atmospheric Sciences. 2nd ed. Elsevier, 627 pp.
- Woods, C., and R. Caballero, 2016: The role of moist intrusions in winter Arctic warming and sea ice decline. *J. Climate*, 29, 4473–4485, https://doi.org/10.1175/JCLI-D-15-0773.1.
- —, —, and G. Svensson, 2013: Large-scale circulation associated with moisture intrusions into the Arctic during winter. *Geophys. Res. Lett.*, **40**, 4717–4721, https://doi.org/10.1002/grl.50912.
- Yao, Y., D. Luo, A. Dai, and I. Simmonds, 2017: Increased quasi stationarity and persistence of winter Ural blocking and Eurasian extreme cold events in response to Arctic warming. Part I: Insights from observational analyses. *J. Climate*, 30, 3549–3568, https://doi.org/10.1175/JCLI-D-16-0261.1.
- Yoo, C., S. Lee, and S. B. Feldstein, 2012a: Arctic response to an MJO-like tropical heating in an idealized GCM. J. Atmos. Sci., 69, 2379–2393, https://doi.org/10.1175/JAS-D-11-0261.1.
- —, —, and —, 2012b: Mechanisms of Arctic surface air temperature change in response to the Madden–Julian oscillation. *J. Climate*, **25**, 5777–5790, https://doi.org/10.1175/JCLI-D-11-00566.1.